Solar Physics (2022) 297:36
https://doi.org/10.1007/s11207-022-01963-0

Observation of a Flare and Filament Eruption in Lyman-α on 8 September 2011 by the *PRoject for OnBoard Autonomy/Large Yield Radiometer* (PROBA2/LYRA)

L. Wauters[1] · M. Dominique[1] · R. Milligan[2] · I.E. Dammasch[1] · M. Kretzschmar[3] · J. Machol[4,5]

Received: 21 April 2021 / Accepted: 7 February 2022

Abstract
The *Large Yield Radiometer* (LYRA) instrument onboard the *PRoject for OnBoard Autonomy* (PROBA2) observes the solar irradiance in four channels in the UV–EUV. One of these channels is centered around the hydrogen line at 121.6 nm. The solar Lyman-α emission line is an optically thick line mostly formed in the chromosphere. Although it is one of the strongest lines of the solar spectrum, only a limited number of instruments provided observations of solar flares in Lyman-α, and those observations differ significantly in shape, durations, and amplitude. We focus on an event that happened on 8 September 2011 (SOL2011-09-08T15:46). This event, an M6.7 flare, was associated with a filament eruption that happened during the decaying phase of the flare. Most of the irradiance fluctuations observed in the Lyman-α time series are synchronized with nonthermal emission fluctuations, as is predicted by flare models. However, there is a late-phase peak in Lyman-α observations that rather correlates with the timing of the filament eruption. We demonstrate that the eruption of the filament is at the origin of this peak.

Keywords Irradiance · Lyman-α · Flare · Filament eruption

This article belongs to the Topical Collection:
PROBA-2 at Ten Years
Guest Editors: Elke D'Huys, Marie Dominique and Matthew J. West

✉ L. Wauters
laurence.wauters@oma.be

[1] SIDC, Royal Observatory of Belgium, 3 Avenue Circulaire, 1180 Uccle, Belgium

[2] Queen's University of Belfast, Belfast, Northern Ireland, UK

[3] LPC2E, UMR 7328 CNRS, University of Orléans, Orléans, France

[4] Cooperative Institute for Research in Environmental Sciences, University of Colorado, Boulder, CO 80309, USA

[5] National Centers for Environmental Information, National Oceanic and Atmospheric Administration, Boulder, CO 80305, USA

Published online: 15 March 2022

1. Introduction

Solar flares, which are among the most powerful events in the solar system, are believed to result from the thermalization of electrons that have been accelerated in the corona during magnetic reconnection. These electrons, when reaching the dense chromosphere, heat up the local plasma, of which the emission suddenly increases. The heated plasma then evaporates filling up the magnetic-loop structures in the flaring region up to the corona. Doing so, it produces irradiance increases over a wide range of wavelengths that reflect the emission temperature reached, and of which the peak is delayed as compared to the peak of the chromospheric emission. Flares are usually observed in the soft X-ray (SXR) and extreme-ultraviolet (EUV) spectral ranges, where the contrast between observations in quiet-Sun and flaring conditions is high. However, solar flares produce increased irradiance throughout the whole solar spectrum. An important amount of energy is dissipated in the ultraviolet above 120 nm (UV) and in the visible range (Woods, Kopp, and Chamberlin, 2006; Kretzschmar, 2011; Milligan et al., 2014). In particular, the hydrogen Lyman-α line at 121.6 nm can radiate up to 100 times more energy during a flare than the SXR (Milligan et al., 2014, 2020; Kretzschmar, 2015). Still, because the quiet-Sun background at this wavelength is much brighter than at the shorter ones (Avrett, Machado, and Kurucz, 1986) and because of instrumental constraints, observations of flares at Lyman-α have for long remained rare, difficult, and often controversial (Milligan and Chamberlin, 2016). Until recently, only a few cases had been reported in the literature, in particular, by Lemaire, Choucq-Bruston, and Vial (1984), Rubio da Costa et al. (2009), Kretzschmar, Dominique, and Dammasch (2013), and Milligan and Chamberlin (2016). However, this wavelength is of prime importance for studying the flare energetics and for understanding the impact of solar activity on the Earth's atmospheric chemistry. Therefore, during the last decade, several missions dedicated to solar observation included a Lyman-α channel. This, in turn, increased the number of available observations. In a recent article, Milligan et al. (2020) compared 477 flares of M- and X-classes observed in both Lyman-α and SXR emissions by the GOES-15 spacecraft. This analysis confirmed that irradiance enhancements up to 10% are detected at Lyman-α in most of the analyzed flares. However, these enhancements are not always in line with those observed in SXR emission. Flares with a large amplitude in the SXR can appear much fainter when observed at Lyman-α, especially when they are located close to the limb. This can be partially explained by the optical thickness of the Lyman-α line. Another article by Jing et al. (2020) used observations by the same instrument to investigate delays between flare peak time in Lyman-α and in the SXR for 658 flares. They concluded that the vast majority of the flares were peaking earlier in Lyman-α than in the SXR, as is expected from chromospheric emission. Still, about a fifth of them were peaking later. Also, for the flares with the Lyman-α emission peaking earlier, they mentioned that a significant portion also displayed secondary subpeaks, of which some were detected during the decaying phase of the flare. The authors attributed these late-phase peaks to thermal emission produced when the heated plasma cools down.

The *Large Yield Radiometer* (LYRA: Hochedez et al., 2006; Dominique et al., 2013) onboard the European Space Agency (ESA) *PRoject for OnBoard Autonomy* (PROBA2) spacecraft is an instrument observing the Sun in four wide bandpasses in the SXR to UV spectral range. One of these channels is centered around the hydrogen Lyman-α line and nominally spans the 120 – 123 nm range. Kretzschmar, Dominique, and Dammasch (2013) reported ten observations of Lyman-α flares by this instrument, most of them happening in 2010. However, as the Lyman-α channel of the nominal unit of this instrument quickly degraded, the detections after 2010 became much rarer. The few cases reported were all

Table 1 Bandwidths associated with each LYRA channel.

Channel	Bandwidth
Lyman-α	120 – 123 nm
Herzberg	190 – 222 nm
Aluminum	0.1 – 5 nm + 17 – 80 nm
Zirconium	0.1 – 2 nm + 6 – 20 nm

obtained when a special observation campaign involving one of the spare units of LYRA was set up (Dominique et al., 2018).

In this article, we report on a new flare observation in the Lyman-α channel of LYRA obtained from the main backup unit of the instrument early in the mission, so as to limit the effects of degradation. This flare has an M6.7 amplitude on the GOES scale and was also seen by the *Geostationary Operational Environmental Satellite* (GOES), the *Extreme Ultraviolet Sensor* (EUVS), and the *Reuven Ramaty High Energy Solar Spectroscopic Imager* (RHESSI). Unfortunately, the *Solar Dynamics Observatory/Extreme Ultraviolet Variability Experiment* (SDO/EVE: Woods et al., 2012), which also has a channel measuring the Lyman-α emission, did not provide any observations of the flare. This event has a late broad peak of smaller amplitude, which occurred about six minutes after the peak time reported in the GOES catalog and which has no counterpart in the SXR. Interestingly, this small and broad peak happens simultaneously with a filament eruption.

In Section 2, we give an overview of instruments involved in this analysis. In Section 3, we provide an analysis of the flare, with an emphasis on its temporal evolution as seen in various bandpasses. The section is also dedicated to the analysis of the small and broad peak, which we associate with the filament eruption that occurred closely after the flare. Section 4 is the conclusion.

2. Instruments

2.1. LYRA

PROBA2 was launched in November 2009, and LYRA measures the solar irradiance at high cadence (nominally 20 Hz) with three redundant units, which can be used either individually or two at a time. Each unit includes the same four broad channels, of which the bandpasses are given in Table 1.

Except for the Lyman-α channel, those bandwidths have been defined so that 95% of the measured signal in quiet-Sun conditions was emitted in the specified spectral range. However, this definition does not apply to the Lyman-α channel, to which out-of-band emission contributes significantly. The purity (i.e. the percentage of the measured signal actually emitted in the defined bandpass) of the backup Lyman-α channel used in this article (corresponding to Unit 3) was estimated at the beginning of the mission at 32.5% only (Benmoussa et al., 2009; Dominique et al., 2013).

The biggest part of the measured quiet-Sun signal originates from wavelengths between 200 and 1000 nm. The spectral response of the main backup Lyman-α channel of LYRA under quiet-Sun conditions is represented in Figure 1. However, during the flares, most of the signal enhancement in this channel comes from the Lyman-α line itself, even if some other flare-sensitive spectral lines in the UV and visible continua are also likely to contribute (Avrett, Machado, and Kurucz, 1986; Dominique et al., 2018). Because the percentage of

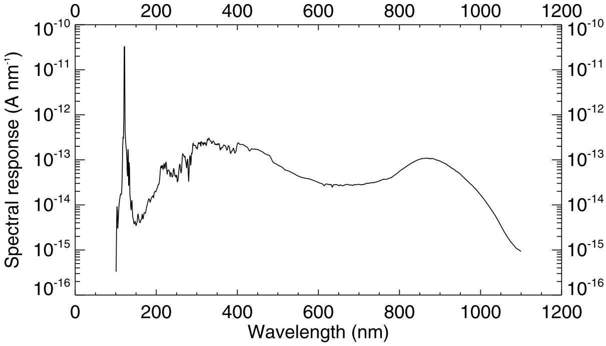

Figure 1 Spectral response of the LYRA Lyman-α channel used in this article when exposed to quiet Sun.

flare emission coming from those other lines is not accurately determinated, we must be very cautious when using the Lyman-α channel of LYRA to estimate the energy dissipated during a flare. Still, a big part of the observed flaring signal in this channel is believed to come from the Lyman-α line itself.

Another instrumental aspect must be considered when working with the Lyman-α channels of LYRA, the aging of the instrument. From the beginning of the mission, LYRA suffered severe degradation, affecting more strongly the longer-wavelength channels of the nominal unit. BenMoussa et al. (2015) attributed this degradation to the progressive deposit of carbon and possibly silicon contaminants. The resulting contaminant layer absorbs the longer wavelengths more than the shorter ones, explaining the different loss of signal in the four channels. In the Lyman-α and Herzberg channels of the nominal unit, the signal fell by 70% within the first month alone, and a loss of 99% is now reached.

If not for its triple redundancy, flare observations with the Lyman-α channel of LYRA would have been limited to 2010. Fortunately, the backup units, which were less frequently opened, degraded much less and were able to observe another few flare events over the mission lifetime.

In this article, we focus on observations made by the main backup unit (Unit 3) on 8 September 2011. At that time the total signal measured by the Lyman-α channel of the main backup unit had decreased by about 30% as compared to the beginning of the mission. However, this drop of signal affected all wavelengths homogeneously. No significant changes have been observed in the channel's spectral response. The LYRA time series used in this article are calibrated using the procedure described by Dominique et al. (2013), which includes a subtraction of the dark current, a scaling to a Sun–spacecraft distance of 1 AU, a correction for the degradation, and a conversion from data numbers to $\mathrm{W\,m^{-2}}$. The time series were also cleaned: maneuvers of the spacecraft (which occur every 25 minutes) and transitions in the South Atlantic Anomaly region were filtered out.

LYRA acquires data at a nominal cadence of 50 ms. However, as the measurements in the Lyman-α channel are very noisy, a one-second rebinning is applied.

2.2. GOES

In this study the LYRA observations are compared to those of the 15th *Geostationary Operational Environmental Satellite* (GOES 15). Each GOES satellite has two X-ray sensors (XRS), which provide solar X-ray fluxes for the wavelength bands of 0.05 to 0.4 nm and 0.1 to 0.8 nm. Measurements in these bands have been made by NOAA satellites since 1974, and the design of the instrument changed little between GOES 1 and GOES 15 (Garcia, 1994; Viereck et al., 2007). Since GOES 13, each spacecraft also carries an *Extreme Ultraviolet Sensor* (EUVS), which measures the solar irradiance in five EUV bands, including one centered on the Lyman-α spectral line.

In this article, we use the data from the EUVS E-channel of GOES 15, which covers the 113 – 130 nm spectral range, with about 88% of the irradiance coming from the Lyman-α line during quiet-Sun conditions. These data are scaled to the daily *SOlar Radiation and Climate Experiment/SOlar Stellar Irradiance Comparison Experiment* (SORCE/SOLSTICE) Lyman-α values with an exponential function, which simultaneously corrects the degradation and the absolute values. GOES/EUVS observations are sampled at a 10.24 second cadence.

2.3. RHESSI

The LYRA observations are also compared with measurements from the *Reuven Ramaty High Energy Solar Spectroscopic Imager* (RHESSI: Lin et al., 2002). RHESSI consists of nine bigrid rotating modulation collimators in front of a spectrometer, from which spatially resolved observations can be produced by post-processing. RHESSI was launched in 2002, and its activity ended in 2018. RHESSI provides information about particle acceleration and explosive energy release in solar flares. The data obtained by this instrument cover the soft X-rays (3 keV) to gamma rays (17 MeV) range. For hard X-ray energies ($\gtrsim$ 50 keV), the emission is typically nonthermal (Krucker, Masuda, and White, 2020).

In this study, we compare the Lyman-α observations of LYRA to the measurements by RHESSI in two energy ranges from 25 to 50 keV and from 50 to 100 keV at the cadence of 4 seconds. These data have been processed with the SolarSoft HESSI routines.

2.4. AIA

The *Atmospheric Imaging Assembly* (AIA) is an instrument onboard the *Solar Dynamics Observatory* (SDO), which has been launched in 2010. AIA provides images from the solar atmosphere in seven wavelengths. In this article, we compare the fluxes measured by LYRA/Lyman-α to the spatially integrated signal from the AIA/30.4 nm and to AIA/160 nm channels. We also check the AIA images at distinct times for the 8 September 2011 event and particularly for the evolution of the filament eruption. The two wavelengths at 160 nm and 30.4 nm, respectively, correspond to emission by the upper photosphere and the chromosphere. We used an AIA temporal sampling of 24 seconds.

3. The M6.7 flare at 16:48 UT

We focus on the observations of 8 September 2011. On that date, a flare campaign was scheduled with the backup Unit 3 of LYRA. Four active regions were present on the visible side of the Sun, among which was the region labeled NOAA 1283 located at N14W40 with a magnetic configuration β-γ-δ, which was very active and produced several M- and X-class flares over a few days. On 8 September 2011, while the LYRA backup unit was operated, the biggest event was an M6.7 flare. It is reported in the GOES catalog to have started at 15:32 UT, reached its peak at 15:46 UT, and ended at 15:52 UT. This flare is illustrated in Figure 2.

As can be seen on this figure, the flare was observed by several instruments. Among others, it produced a clear signature in the Lyman-α channel of LYRA. As mentioned before,

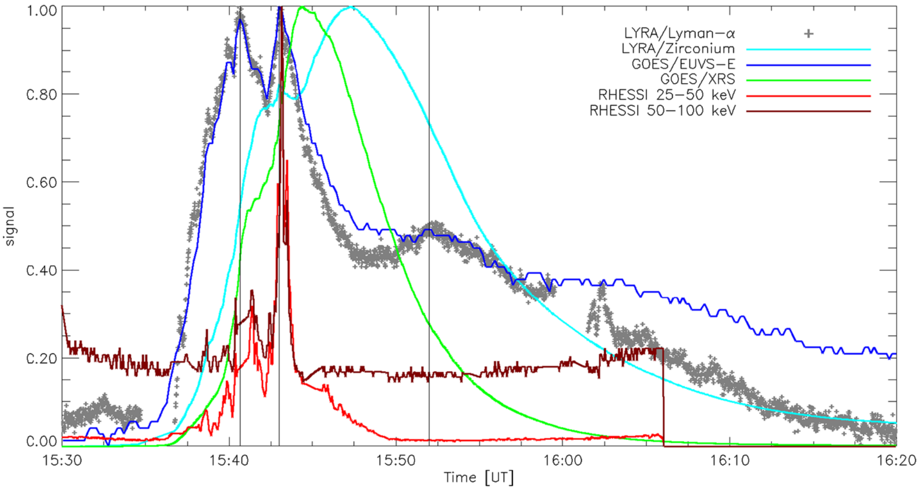

Figure 2 The M6.7 flare on 8 September 2011, as observed by the Lyman-α channel of LYRA (*gray crosses*), the Zirconium channel of LYRA (*cyan*), the E channel of GOES/EUVS (*dark blue*), the 0.1 – 0.8 nm channel of GOES/XRS (*green*), the 25 – 50 keV range by RHESSI (*red*), and the 50 – 100 keV range by RHESSI (*brown*). Unity-based normalization is used for all curves over the flare duration, which removes the preflare background contribution.

the data samples acquired by this instrument during spacecraft maneuvers were filtered out, producing the gaps around 15:35 UT and 16:00 UT, which unfortunately mask the start of the flare. However, this flare was also observed by GOES/EUVS-E. The consistency between the Lyman-α observations by GOES and LYRA is good, despite the fact that the two instruments have different spectral responses. We find the Pearson correlation coefficient 0.954 between the two signals (after interpolation of the GOES/EUVS-E signal to the LYRA times) for the whole time range and the correlation coefficient 0.984 for the impulsive phase only (15:36 UT to 15:43 UT). This could be an argument supporting the fact that most of the emission in this range of the solar spectrum during flares comes from the Lyman-α line itself. It also demonstrates that the limited degradation affecting the backup unit of LYRA did not significantly change the bandpass of the Lyman-α channel at the moment of the flare. One noticeable difference between the two instruments is that the ten-second cadence of GOES/EUVS-E tends to smear out the short-timescale fluctuations, which are better visible in LYRA data. The LYRA temporal profile also shows slightly faster cooling during the decaying phase of the flare than that in GOES, which might reflect the contribution to the LYRA broader passband of emission lines formed at higher temperatures and cooling quicker, such as the Si IV lines around 140 nm and the C IV lines around 155 nm.

The absolute amplitude of the flare also differs in the two instruments. LYRA/Lyman-α shows an increase by 0.45% of its preflare measured irradiance, corresponding to a flare increase of 2.8×10^{-5} Wm^{-2}, which is of the same order as the amplitude of the other 11 flares observed by LYRA/Lyman-α by Kretzschmar, Dominique, and Dammasch (2013). On the other hand, a much more significant increase by 10.26%, corresponding to 7.2×10^{-4} Wm^{-2}, is observed by GOES/EUVS-E, consistently with the study of Milligan et al. (2020). The difference in amplitude is not completely understood. To check if it could be partially explained by the degradation of the LYRA instrument, even if this was still limited at the time of the flare, we simulated the increase of signal that should be detected by LYRA and compared it to the measured one. The simulation only covered the 1 – 190 nm

Table 2 Times of the three main peaks as observed in the various datasets.

Instrument	First peak time [UT]	Second peak time [UT]	Third peak time [UT]
GOES/XRS	15:41	15:46	-
LYRA/Zirconium	15:42	15:47	-
LYRA/Lyman-α	15:41	15:43	15:52
GOES/EUVS-E	15:41	15:43	15:52
RHESSI 12 – 25 keV	15:41	15:43	-
RHESSI 25 – 50 keV	15:41	15:43	-

range[1] and was performed by multiplying solar spectra obtained from the FISM2 model (Chamberlin et al., 2020) at the peak time and before the flare (at, respectively, 15:43 UT and 15:30 UT) by the responsivity of the instrument and integrating their emission over the bandpass. It resulted in an expected increase of signal of 4×10^{-6} Wm^{-2}, which is lower but still consistent with the LYRA observations. This tends to confirm that the impact of degradation on LYRA measurements at the time of the flare is limited. Other possible sources for the difference in flare amplitude measured by LYRA and GOES could be the bandpass of the two instruments with different flare-sensitive spectral lines other than Lyman-α contributing to the measured signal. The authors have also considered the impact of geocoronal absorption, as the orbit of PROBA2 has a much lower altitude than that of GOES (700 km versus 36,000 km). Still, a factor of 20 difference seems surprising.

In Figure 2, two main peaks can be identified between 15:35 UT and 15:50 UT in most time series. This double-peak profile, which is particularly pronounced in Lyman-α observations, corresponds to two main heating episodes also visible in the HXR curves (although a short data gap masks the first peak in RHESSI data). This two-step heating profile is in fact also present in the SXR measurements, even if the first one is not associated with a peak strictly speaking, but rather to a bump around 15:42 UT. The times of the maximum of each heating episode are indicated in the second and third columns of Table 2.

From Figure 2 we can also see that the time of the flare peak differs for each wavelength range. The Zirconium time series of LYRA peaks later than that from GOES/XRS, as it corresponds to emission by coronal plasma with lower temperature. Conversely, the observations in Lyman-α peak three minutes earlier. Such a behavior is characteristic of the chromospheric flare emission, which is expected to directly track the nonthermal emission. The Lyman-α emission is indeed produced when the nonthermal electrons accelerated during the magnetic reconnection and that produce HXR via brehmstrahlung reach the chromosphere and transfer their energy to the local plasma (see, e.g., Milligan and Chamberlin, 2016). This is confirmed by a good synchronization of the Lyman-α observations with those made in HXR by RHESSI in two energy ranges, 25 – 50 keV and 50 – 100 keV.

Note that if all the small-scale fluctuations in the Lyman-α observations correlate well with those in the nonthermal emission measured by RHESSI, the overall flare profile is much smoother in Lyman-α than in HXR, with a long rise-then-decay background extending beyond the impulsive phase of the flare, which is more typical of thermal emission. Part of this contribution could be emitted higher up in the corona by the flaring loops, rather than at the footpoints during the chromospheric evaporation.

[1] The limitation to 190 nm was dictated by the spectral coverage of the FISM 2 model. However, this spectral range includes, following the CHIANTI atomic database, the main spectral lines contributing to flares in the bandpass of the Lyman-α channel of LYRA.

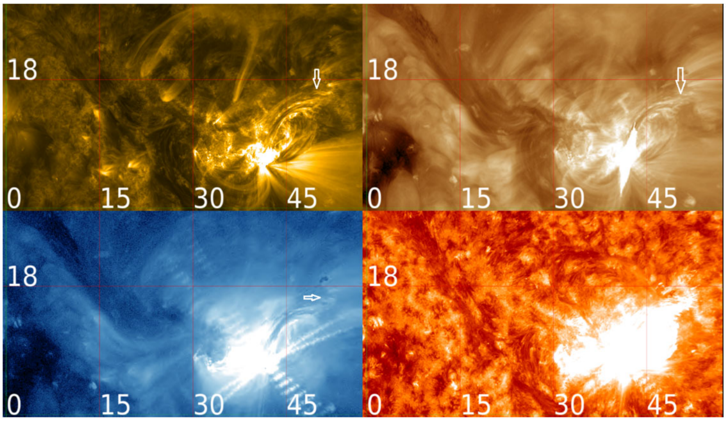

Figure 3 The eruption of the filament (*shown by arrows*) as observed at 15:53 UT by AIA 17.1 (*top-left panel*), 19.3 (*top-right panel*), 33.5 (*bottom-left panel*), and 30.4 nm (*bottom-right panel*). *Degrees are used for axis units*.

All in all, the sequence of peak times in the various channels follows the predictions of the standard flare model and the Neupert effect (Neupert, 1968).

However, something more unusual can also be observed in Figure 2. Around 15:53 UT, the Lyman-α curve of LYRA exhibits a broad third peak of lower amplitude than the first two, which is also visible in GOES/EUVS-E (although less prominent), but which is not visible in other channels. We could not relate this peak to any instrumental or in-situ cause (such as the impact of a particle on the detector in the South Atlantic Anomaly), in which case it would have affected other channels of LYRA that share the same detector technology.

One possible explanation for this late third peak in Lyman-α is that it corresponds to thermal emission produced by the plasma that has been heated during the impulsive phase of the flare and has "evaporated" in the flare loops in the corona, as it cools down to chromospheric temperatures. Jing et al. (2020), reported that about a fifth of the flares have Lyman-α emission that peaks after the SXR peak, which they attributed to such coronal emission. The delay of about nine minutes was observed between the second peak, and this third one in Lyman-α would be compatible with this explanation.

However, this third peak might have another origin, a filament from the same active region that partially erupted at the same moment and that was described by Zhang et al. (2015). The filament eruption was visible in various wavelengths, as illustrated on Figure 3, produced using JHelioviewer (Müller et al., 2017). As was described in this article, the filament started to rise around 15:30 UT. It started to broaden at 15:42:30 UT, and at 15:46 UT it split into two parts, one of which fell back on the Sun. The other one, however, managed to escape around 15:55 UT and created a faint CME detected by SOHO/LASCO (see cdaw.gsfc.nasa.gov/CME_list/) around 16:48 UT.

The third peak in the LYRA Lyman-α series covers the 15:46 UT to 16:00 UT time range, which matches the interval during which the filament starts to thicken until the moment its failing part falls back on the Sun.

Detection of filament eruptions have been rarely reported in Lyman-α. Rubio da Costa et al. (2009) detected Lyman-α emission during an eruption that occurred on 8 September 1999. However, as this eruption was characterized by both a flare and a filament eruption, it was not clear whether the Lyman-α emission was produced by cool material possibly mixed

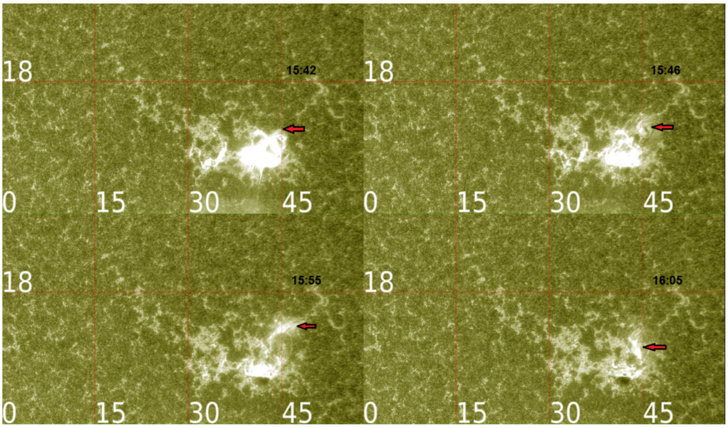

Figure 4 The eruption of the filament as observed by AIA 160.0 nm. The *arrows show the part of the filament that fell back on the Sun. The axis units are in degrees.*

with hotter one in the filament or whether this was flare emission scattered by the filament material.

Milligan (2021) also attributed to a failed filament eruption the unusual high amplitude of Lyman-α emission observed by GOES during a C6.6 flare that happened on 17 February 2014. Despite its large amplitude, the Lyman-α emission during this flare was also characterized by a profile more similar to SXR emission than to HXR emission. All this seemed to point to a coronal origin of this Lyman-α emission.

In our case the Lyman-α profile during the third peak is rather smooth and does not have any counterpart in the HXR. To confirm its origin, we looked for spatially resolved observations of that event. There are, to our knowledge, no images of this event in Lyman-α. However, this filament eruption is clearly visible in AIA 160 nm, which also corresponds to emission by the transition region. The part of the filament that falls back on the Sun appears clearly in emission, as can be seen in Figure 4.

By summing up the irradiance of all AIA pixels we can produce an irradiance time series of AIA measurements. In AIA 160 nm a small bump is present around 15:53 UT, which is well synchronized with that in Lyman-α (see Figure 5). The same exercise with AIA 30.4 nm observations, which corresponds to higher emission temperatures, is not conclusive.

The fact that the filament eruption is not seen in the time series corresponding to the emission by hotter plasma may provide us with an indication about the temperature reached during the filament eruption.

To better assess the origin of the third peak, we have repeated the summation of pixels intensities over two selected areas of AIA 160 nm images, respectively corresponding to the flare core and to the filament, as illustrated on the left part of Figure 6. The corresponding lightcurves for the flare and for the filament are shown on the right part of the same figure. The filament lightcurve has a large broad peak, which coincides with the third peak observed in LYRA/Lyman-α.

4. Conclusions

In this article, we presented a new observation of an eruption observed in Lyman-α by both PROBA2/LYRA and GOES/EUVS-E. This eruption was associated with an M6.7 flare that

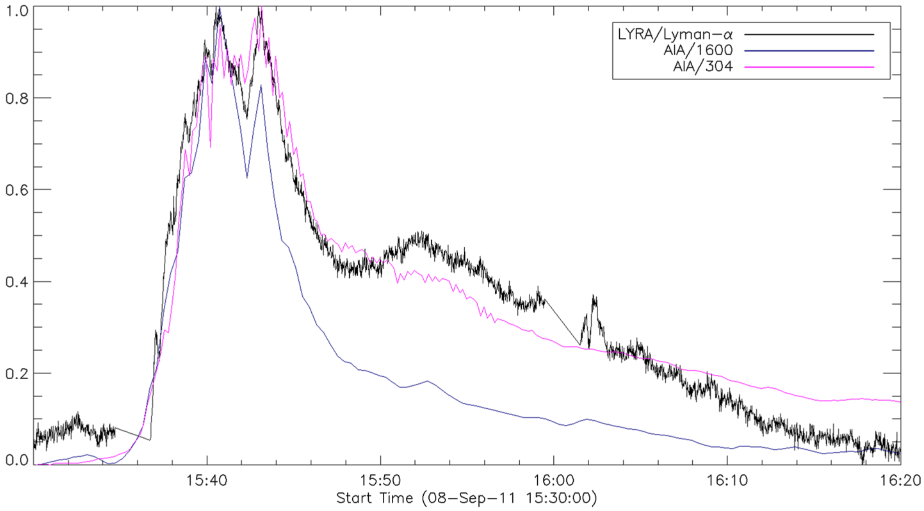

Figure 5 Comparison of the normalized irradiance variation in LYRA/Lyman-α (*black*), AIA 160 nm (*blue*), and AIA 30.4 nm (*pink*).

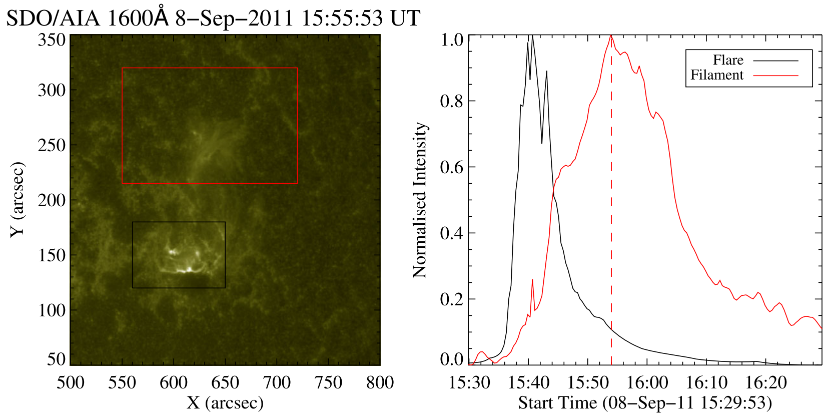

Figure 6 The *left panel* shows the regions corresponding to the flare (*white-square*) and to the filament (*red-square*) as observed at 15:55 by AIA 160.0 nm. The *right panel* shows the time series corresponding, respectively, to the flare (*white*) and filament (*red*) integrated intensities.

happened on 8 September 2011. In this specific case, most of the Lyman-α emission exhibits a profile with two main peaks tracking nonthermal emission and peaking ahead of the SXRs, as expected. However, a third, lower and broad peak was observed around 15:52 UT, i.e., respectively 11 minutes after the first peak and 9 minutes after the second one. We have shown that a failed filament eruption is at the origin of this third peak.

A fifth of flares observed in Lyman-α seem to peak after the SXR emission. We believe that it would be also interesting to search those for the presence of filament eruption. This will be done in future work.

Acknowledgments LYRA is a project of the Centre Spatial de Liège, the Physikalisch-Meteorologisches Observatorium Davos, and the Royal Observatory of Belgium funded by the Belgian Federal Science Policy Office (BELSPO) and by the Swiss Bundesamt für Bildung und Wissenschaft. R. Milligan would like to thank The Sciences and Technologies Council (UK) for the award of an Ernest Rutherford Fellowship (ST/N004981/2).

Funding statement L. Wauters and M. Dominique thank the European Space Agency (ESA) and BELSPO for their support in the framework of the PRODEX Programme.

Data Availability The LYRA data used in this article are available from the author on request by email; a full LYRA archive is available from the PROBA2 website (proba2.sidc.be/data/LYRA).

Declarations

Disclosure of Potential Conflicts of Interest The authors declare that they have no conflict of interest.

References

Avrett, E.H., Machado, M.E., Kurucz, R.L.: 1986, Chromospheric flare models. In: Neidig, D.F. (ed.) *The Lower Atmosphere of Solar Flares, NSO, Sunspot NM*, 216. ADS.

Benmoussa, A., Dammasch, I.E., Hochedez, J.-F., Schühle, U., Koller, S., Stockman, Y., Scholze, F., Richter, M., Kroth, U., Laubis, C., Dominique, M., Kretzschmar, M., Mekaoui, S., Gissot, S., Theissen, A., Giordanengo, B., Bolsee, D., Hermans, C., Gillotay, D., Defise, J.-M., Schmutz, W.: 2009, Pre-flight calibration of LYRA, the solar VUV radiometer on board PROBA2. *Astron. Astrophys.* **508**, 1085. DOI. ADS.

BenMoussa, A., Giordanengo, B., Gissot, S., Dammasch, I.E., Dominique, M., Hochedez, J.-F., Soltani, A., Bourzgui, N., Saito, T., Schühle, U., Gottwald, A., Kroth, U., Jones, A.R.: 2015, Degradation assessment of LYRA after 5 years on orbit - Technology Demonstration -. *Exp. Astron.* **39**, 29. DOI. ADS.

Chamberlin, P.C., Eparvier, F.G., Knoer, V., Leise, H., Pankratz, A., Snow, M., Templeman, B., Thiemann, E.M.B., Woodraska, D.L., Woods, T.N.: 2020, The flare irradiance spectral model-version 2 (FISM2). *Space Weather* **18**, e02588. DOI. ADS.

Dominique, M., Hochedez, J.-F., Schmutz, W., Dammasch, I.E., Shapiro, A.I., Kretzschmar, M., Zhukov, A.N., Gillotay, D., Stockman, Y., BenMoussa, A.: 2013, The LYRA instrument onboard PROBA2: description and in-flight performance. *Solar Phys.* **286**, 21. DOI. ADS.

Dominique, M., Zhukov, A.N., Heinzel, P., Dammasch, I.E., Wauters, L., Dolla, L., Shestov, S., Kretzschmar, M., Machol, J., Lapenta, G., Schmutz, W.: 2018, First detection of solar flare emission in mid-ultraviolet Balmer continuum. *Astrophys. J. Lett.* **867**, L24. DOI. ADS.

Garcia, H.A.: 1994, Temperature and emission measure from Goes soft X-ray measurements. *Solar Phys.* **154**, 275. DOI. ADS.

Hochedez, J.-F., Schmutz, W., Stockman, Y., Schühle, U., Benmoussa, A., Koller, S., Haenen, K., Berghmans, D., Defise, J.-M., Halain, J.-P., Theissen, A., Delouille, V., Slemzin, V., Gillotay, D., Fussen, D., Dominique, M., Vanhellemont, F., McMullin, D., Kretzschmar, M., Mitrofanov, A., Nicula, B., Wauters, L., Roth, H., Rozanov, E., Rüedi, I., Wehrli, C., Soltani, A., Amano, H., van der Linden, R., Zhukov, A., Clette, F., Koizumi, S., Mortet, V., Remes, Z., Petersen, R., Nesládek, M., D'Olieslaeger, M., Roggen, J., Rochus, P.: 2006, LYRA, a solar UV radiometer on Proba2. *Adv. Space Res.* **37**, 303. DOI. ADS.

Jing, Z., Pan, W., Yang, Y., Song, D., Tian, J., Li, Y., Cheng, X., Hong, J., Ding, M.D.: 2020, The Lyα emission in solar flares. I. A statistical study on its relationship with the 1 – 8 Å Soft X-ray emission. *Astrophys. J.* **904**, 41. DOI. ADS.

Kretzschmar, M.: 2011, The Sun as a star: observations of white-light flares. *Astron. Astrophys.* **530**, A84. DOI. ADS.

Kretzschmar, M.: 2015, Temperature dependence of the flare fluence scaling exponent. *Solar Phys.* **290**, 3593. DOI. ADS.

Kretzschmar, M., Dominique, M., Dammasch, I.E.: 2013, Sun-as-a-star observation of flares in Lyman α by the PROBA2/LYRA radiometer. *Solar Phys.* **286**, 221. DOI. ADS.

Krucker, S., Masuda, S., White, S.M.: 2020, Microwave and hard X-ray flare observations by NoRH/NoRP and RHESSI: peak-flux correlations. *Astrophys. J.* **894**, 158. DOI. ADS.

Lemaire, P., Choucq-Bruston, M., Vial, J.-C.: 1984, Simultaneous H and K Ca ii, h and k Mg ii, Lα and Lα H i profiles of the April 15, 1978 solar flare observed with the OSO-8/L.P.S.P. experiment. *Solar Phys.* **90**, 63. DOI. ADS.

Lin, R.P., Dennis, B.R., Hurford, G.J., Smith, D.M., Zehnder, A., Harvey, P.R., Curtis, D.W., Pankow, D., Turin, P., Bester, M., Csillaghy, A., Lewis, M., Madden, N., van Beek, H.F., Appleby, M., Raudorf, T., McTiernan, J., Ramaty, R., Schmahl, E., Schwartz, R., Krucker, S., Abiad, R., Quinn, T., Berg, P., Hashii, M., Sterling, R., Jackson, R., Pratt, R., Campbell, R.D., Malone, D., Landis, D., Barrington-Leigh, C.P., Slassi-Sennou, S., Cork, C., Clark, D., Amato, D., Orwig, L., Boyle, R., Banks, I.S., Shirey, K., Tolbert, A.K., Zarro, D., Snow, F., Thomsen, K., Henneck, R., McHedlishvili, A., Ming, P., Fivian, M., Jordan, J., Wanner, R., Crubb, J., Preble, J., Matranga, M., Benz, A., Hudson, H., Canfield, R.C., Holman, G.D., Crannell, C., Kosugi, T., Emslie, A.G., Vilmer, N., Brown, J.C., Johns-Krull, C., Aschwanden, M., Metcalf, T., Conway, A.: 2002, The Reuven Ramaty High-Energy Solar Spectroscopic Imager (RHESSI). *Solar Phys.* **210**, 3. DOI. ADS.

Milligan, R.O.: 2021, Solar irradiance variability due to solar flares observed in Lyman-alpha emission. *Solar Phys.* **296**, 51. DOI. ADS.

Milligan, R.O., Chamberlin, P.C.: 2016, Anomalous temporal behaviour of broadband Ly α observations during solar flares from SDO/EVE. *Astron. Astrophys.* **587**, A123. DOI. ADS.

Milligan, R.O., Kerr, G.S., Dennis, B.R., Hudson, H.S., Fletcher, L., Allred, J.C., Chamberlin, P.C., Ireland, J., Mathioudakis, M., Keenan, F.P.: 2014, The radiated energy budget of chromospheric plasma in a major solar flare deduced from multi-wavelength observations. *Astrophys. J.* **793**, 70. DOI. ADS.

Milligan, R.O., Hudson, H.S., Chamberlin, P.C., Hannah, I.G., Hayes, L.A.: 2020, Lyman-alpha variability during solar flares over Solar Cycle 24 using GOES-15/EUVS-E. *Space Weather* **18**, e02331. DOI. ADS.

Müller, D., Nicula, B., Felix, S., Verstringe, F., Bourgoignie, B., Csillaghy, A., Berghmans, D., Jiggens, P., García-Ortiz, J.P., Ireland, J., Zahniy, S., Fleck, B.: 2017, JHelioviewer. Time-dependent 3D visualisation of solar and heliospheric data. *Astron. Astrophys.* **606**, A10. DOI. ADS.

Neupert, W.M.: 1968, Comparison of solar X-ray line emission with microwave emission during flares. *Astrophys. J.* **153**, L59. DOI. ADS.

Rubio da Costa, F., Fletcher, L., Labrosse, N., Zuccarello, F.: 2009, Observations of a solar flare and filament eruption in Lyman α and X-rays. *Astron. Astrophys.* **507**, 1005. DOI. ADS.

Viereck, R., Hanser, F., Wise, J., Guha, S., Jones, A., McMullin, D., Plunket, S., Strickland, D., Evans, S.: 2007, Solar extreme ultraviolet irradiance observations from GOES: design characteristics and initial performance. In: Fineschi, S., Viereck, R.A. (eds.) *Sol. Phys. and Space Weather Instrumentation II*, *Soc. Photo-Opt. Instrument Eng. (SPIE)* **CS-6689**, 66890K. DOI. ADS.

Woods, T.N., Kopp, G., Chamberlin, P.C.: 2006, Contributions of the solar ultraviolet irradiance to the total solar irradiance during large flares. *J. Geophys. Res.* **111**, A10S14. DOI. ADS.

Woods, T.N., Eparvier, F.G., Hock, R., Jones, A.R., Woodraska, D., Judge, D., Didkovsky, L., Lean, J., Mariska, J., Warren, H., McMullin, D., Chamberlin, P., Berthiaume, G., Bailey, S., Fuller-Rowell, T., Sojka, J., Tobiska, W.K., Viereck, R.: 2012, Extreme Ultraviolet Variability Experiment (EVE) on the Solar Dynamics Observatory (SDO): overview of science objectives, instrument design, data products, and model developments. *Solar Phys.* **275**, 115. DOI. ADS.

Zhang, Q.M., Ning, Z.J., Guo, Y., Zhou, T.H., Cheng, X., Ji, H.S., Feng, L., Wiegelmann, T.: 2015, Multiwavelength observations of a partially eruptive filament on 2011 September 8. *Astrophys. J.* **805**, 4. DOI. ADS.